

REPORTS

Figure 1 shows that CH₄ and N₂O varied together not only on orbital time scales (the clear precessional signal and slower variations), but also on millennial time scales during the Younger Dryas, Dansgaard/Oeschger interstadial 8, and other events between about 40 and 90 ka. This observation is consistent with monsoonal coupling of terrestrial and marine realms. During periods of increased monsoonal activity (interstadial periods), enhanced upwelling of nutrient-rich water in the Arabian Sea and the Eastern Tropical Pacific supported increased marine productivity and thus increased organic-matter rain. The enhanced flux of organic matter caused a reduction in mid-water oxygen concentration, thereby increasing denitrification; a consequent increase in N₂O production ultimately led to increased N₂O emissions in upwelling areas modulated by monsoonal circulation patterns (33, 34). At the same time, enhanced monsoonal rainfall would have expanded the region of wet soils producing CH₄ and N₂O.

One notable exception to the general CH₄/N₂O correspondence occurs during the cooling event that began about 80 ka. N₂O levels remained high for ~7 ky after CH₄ levels dropped precipitously. Perhaps during this period, the CH₄/N₂O temporal relation may reflect greater initial sensitivity of CH₄ emissions to terrestrial drying. Complete soil saturation optimizes CH₄ production, whereas reduced N₂O emissions from drying of some regions below the 60 to 90% saturated window for optimal N₂O production are partially offset by drying of wetter areas into the optimum N₂O emission window. Additionally, because high northern latitudes were more important for CH₄ [~18% of preanthropogenic CH₄ emissions in latitude bands north of 40°N (8)] than for N₂O [~9% (35)], ice-sheet advance may have impacted CH₄ emissions more directly and quickly than N₂O emissions. Additional isotopic analyses on samples before 30 ka might clarify the relative roles of marine and terrestrial sources of N₂O in these cases, and why this behavior is not shown strongly at other times.

References and Notes

- Current N₂O emissions from the terrestrial biosphere are estimated to be 12 ± 3 Tg N/year, and preanthropogenic estimates are ~7 Tg N/year (12, 36–39). Marine N₂O emissions are estimated to be 4 ± 2 Tg N/year (40, 41). About 98% of the total atmospheric N₂O sink occurs in the stratosphere. Minschwaner et al. (42) estimated the 1980 value to be 12 ± 4 Tg N/year, corresponding to a mean atmospheric lifetime of 118 ± 25 years (43).
- J. R. Holton et al., *Rev. Geophys.* **33**, 403 (1995).
- J. Fluckiger et al., *Science* **285**, 227 (1999).
- J. Fluckiger et al., *Global Biogeochem. Cycles* **16**, 1010, doi:10.1029/2001GB001417 (2002).
- M. Leuenberger, U. Siegenthaler, *Nature* **360**, 449 (1992).
- P. Martinerie, G. P. Brasseur, C. Granier, *J. Geophys. Res.* **100**, 14291 (1995).
- P. Crutzen, C. Bruhl, *Geophys. Res. Lett.* **20**, 1047 (1993).
- J. A. Chappellaz, I. Y. Fung, A. M. Thompson, *Tellus* **45B**, 228 (1993).
- J. Chappellaz et al., *Nature* **366**, 443 (1993).
- E. Brook, T. Sowers, J. Orchardo, *Science* **273**, 1087 (1996).
- A. F. Bouwman, I. Fung, E. Matthews, J. John, *Global Biogeochem. Cycles* **7**, 557 (1993).
- E. A. Davidson, in *Biogeochemistry and Global Change, Radiatively Active Trace Gases* R. S. Oremland, Ed. (Chapman & Hall, New York, 1993), pp. 369–386.
- J. Jubenville, thesis, Pennsylvania State University (2000).
- T. A. Sowers, J. Jubenville, *J. Geophys. Res.* **105**, 29155 (2000).
- T. Sowers, *J. Geophys. Res.* **106**, 31903 (2001).
- E. J. Brook, S. Harder, J. Severinghaus, E. Steig, C. Sucher, *Global Biogeochem. Cycles* **14**, 559 (2000).
- T. A. Sowers, M. L. Bender, D. Raynaud, *J. Geophys. Res.* **94**, 5137 (1989).
- C. M. Trudinger et al., *J. Geophys. Res.* **102**, 6747 (1997).
- T. Blunier, E. Brook, *Science* **291**, 109 (2001).
- A. J. Gow et al., *J. Geophys. Res.* **102**, 26559 (1997).
- A. Indermuhle, E. Monnin, B. Stauffer, T. Stocker, M. Wahlen, *Geophys. Res. Lett.* **27**, 735 (2000).
- A. Indermuhle et al., *Nature* **398**, 121 (1999).
- H. J. Smith, H. Fischer, M. Wahlen, D. Mastroianni, B. Deck, *Science* **400**, 248 (1999).
- M. L. Bender, B. Malize, J. Orchardo, T. Sowers, J. Jouzel, in *Mechanisms of Global Climate Change at Millennial Time Scales*, P. U. Clark, R. S. Webb, L. D. Keigwin, Eds. (American Geophysical Union, Washington, DC, 2000), American Geophysical Union Monograph 112, pp. 149–165.
- T. Rahn, M. Wahlen, *Global Biogeochem. Cycles* **14**, 537 (2000).
- T. Sowers, A. Rodebaugh, N. Yoshida, S. Toyoda, *Global Biogeochem. Cycles* **16**, 1129, doi:10.1029/2002GB001911 (2002).
- B. Goldstein, F. Joos, T. Stocker, *Geophys. Res. Lett.* **30**, 1092, doi:10.1029/2002GL016418 (2003).
- J. H. Butler, J. W. Elkins, T. M. Thompson, D. B. Egan, *J. Geophys. Res.* **94**, 14865 (1989).
- D. M. Sigman, E. A. Boyle, *Nature* **407**, 859 (2000).
- R. Archer, A. Winguth, D. Lea, N. Mahowald, *Rev. Geophys.* **38**, 159 (2000).
- S. P. Seitzinger, C. Kroeze, *Global Biogeochem. Cycles* **12**, 93 (1998).
- H. W. Bange, S. Rapsomanikis, M. O. Andreae, *Global Biogeochem. Cycles* **10**, 197 (1996).
- M. A. Altabet, M. J. Higginson, D. W. Murray, *Nature* **415**, 159 (2002).
- A. Suthhof, V. Ittekkot, B. Gaye-Haake, *Global Biogeochem. Cycles* **15**, 637 (2001).
- A. F. Bouwman, K. W. Van der Hoeck, J. G. J. Olivier, *J. Geophys. Res.* **100**, 2785 (1995).
- C. S. Potter, P. A. Matson, P. M. Vitousek, E. A. Davidson, *J. Geophys. Res.* **101**, 1361 (1996).
- C. S. Potter, S. A. Klooster, *Global Biogeochem. Cycles* **12**, 621 (1998).
- E. A. Davidson, in *Microbial Production and Consumption of Greenhouse Gases: Methane, Nitrogen Oxides and Halomethanes*, J. E. Rogers, W. B. Whitman, Eds. (American Society for Microbiology, Washington, DC, 1991), pp. 219–235.
- C. Kroeze, A. Mosier, L. Bouman, *Global Biogeochem. Cycles* **13**, 1 (1999).
- C. Nevison, R. F. Weiss, D. J. I. Erickson, *J. Geophys. Res.* **100**, 15809 (1995).
- J. E. Dore, B. N. Popp, D. M. Karl, F. J. Sansone, *Nature* **396**, 63 (1998).
- K. Minschwaner, R. J. Salawitch, M. B. McElroy, *J. Geophys. Res.* **98**, 10543 (1993).
- K. Minschwaner, R. W. Carver, B. P. Briegleb, A. E. Roche, *J. Geophys. Res.* **103**, 23243 (1998).
- A. Berger, M. F. Loutre, *Quat. Sci. Rev.* **10**, 297 (1991).
- P. M. Grootes, M. Stuiver, J. W. C. White, S. Johnsen, J. Jouzel, *Nature* **366**, 552 (1993).
- J. M. Barnola, D. Raynaud, Y. S. Korotkevich, C. Lorius, *Nature* **329**, 408 (1987).
- Supported by NSF—Office of Polar Programs (grants 9526556 to T.A.S. and 0087160 and 0126187 to R.B.A.). Special thanks to K. Keller, R. Najjar, J. Fluckiger, and two anonymous reviewers who greatly improved the manuscript.

Supporting Online Material

www.sciencemag.org/cgi/content/full/301/5635/945/DC1
SOM Text
Reference

3 April 2003; accepted 8 July 2003

340,000-Year Centennial-Scale Marine Record of Southern Hemisphere Climatic Oscillation

Katharina Pahnke,^{1*} Rainer Zahn,^{1,2*} Henry Elderfield,³ Michael Schulz⁴

In order to investigate rapid climatic changes at mid-southern latitudes, we have developed centennial-scale paleoceanographic records from the southwest Pacific that enable detailed comparison with Antarctic ice core records. These records suggest close coupling of mid-southern latitudes with Antarctic climate during deglacial and interglacial periods. Glacial sections display higher variability than is seen in Antarctic ice cores, which implies climatic decoupling between mid- and high southern latitudes due to enhanced circum-Antarctic circulation. Structural and temporal similarity with the Greenland ice core record is evident in glacial sections and suggests a degree of interhemispheric synchrony not predicted from bipolar ice core correlations.

Climatic instability and abrupt changes are recognized features of the last glacial period and have been found in climate archives worldwide (1–6). To date, the best-resolved records of changes in the Southern Hemisphere are from Antarctic ice cores (5, 6). The dearth of continuous high-resolution pa-

leo-climatic records from mid- and high southern latitudes precludes the tracing of climatic signals from Antarctic records to the extra-polar Southern Hemisphere. This highlights the importance of establishing fine-scale marine records that enable the mapping of millennial to submillennial climatic chang-

es across southern latitudes, which is necessary for constructing a coherent picture of interhemispheric climate patterns. Here we present sea surface temperature (SST) and stable oxygen isotope ($\delta^{18}\text{O}$) records from a marine sediment core that span the past three climatic cycles and resolve mid-southern latitude climate variability at a temporal resolution close to, and in some sections higher than, the Antarctic Vostok climate record.

Thirty-six-meter-long IMAGES (International Marine Past Global Changes Studies) (7) core MD97-2120 was retrieved from Chattham Rise, east of New Zealand ($45^{\circ}32.06'S$, $174^{\circ}55.85'E$; water depth, 1210 m). The hydrography at the core site is controlled by the Subtropical Convergence (STC), which lies immediately to the north, separating warm, saline, subtropical surface waters from colder, fresher subantarctic waters (8). We established centennial-scale records of planktonic foraminiferal (*Globigerina bulloides*) $\delta^{18}\text{O}$ ($\delta^{18}\text{O}_{\text{plk}}$) and Mg/Ca ratios (9) that reflect surface water hydrographic changes over the past 340,000 years.

An age scale has been established for the records through the application of a series of iterative steps. The age of the upper core section (0 to 10.6 m) is constrained by 13 accelerator mass spectrometry (AMS) ^{14}C dates and by the Kawakawa ash [radiocarbon age, 22.59 thousand years (ky); equivalent calendar-year age, 26.17 ky (10, 11)]. The ^{14}C ages between 0 and 20 ky were converted to calendar ages using the marine calibration data set (12), together with a local reservoir age anomaly of 240 ± 40 years (13). AMS ages between 26.6 and 32.3 ky were reservoir-corrected by 640 years and converted into calendar years using a marine ^{14}C -versus-calendar year correlation that traces geomagnetic paleointensity variations (9, 14, 15). To further constrain our age model, we measured a fine-scale benthic $\delta^{18}\text{O}$ section that was correlated with the glacial $\delta^{18}\text{O}$ section of core MD95-2042 in the northeast Atlantic (9, 16) in the interval from 40 to 72 ky. The chronology of core MD95-2042, through its $\delta^{18}\text{O}_{\text{plk}}$, is tied to the Greenland Ice Sheet Project 2 (GISP2) time scale (16). The glacial section of the benthic $\delta^{18}\text{O}$ record of core MD95-2042 mimics the structure of the Antarctic Vostok ice core deuterium (δD) record (16), which is also

seen in our benthic $\delta^{18}\text{O}$ record, thus allowing the transfer of the Greenland ice core chronology from core MD95-2042 to our records. The age scale for the lower part of the core, below 10.6 m, is derived from the correlation of our Mg/Ca-derived SST ($\text{SST}_{\text{Mg/Ca}}$) record with the Antarctic Vostok δD atmospheric temperature record on its orbitally tuned age scale (17). We used the lower-resolution $\text{SST}_{\text{Mg/Ca}}$ record for this correlation, because $\delta^{18}\text{O}_{\text{plk}}$ combines local hydrological and global ice volume effects that impede a firm correlation with Antarctic temperature. According to the age model, sedimentation rates along core MD97-2120 are between 15.5 cm/ky during glacial and 6 cm/ky during interglacials. Mean time steps along the $\delta^{18}\text{O}_{\text{plk}}$ and Mg/Ca records are 192 ± 83 years (at a 2-cm sampling interval) and 931 ± 405 years (at a 10-cm sampling interval). The resolution of the $\delta^{18}\text{O}_{\text{plk}}$ record is close to that of the Vostok δD record (time step, 126 ± 100 years). In the lower sections, beyond ~ 230 ky,

the resolution of $\delta^{18}\text{O}_{\text{plk}}$ is the same as and higher than in the Vostok record.

Mg/Ca signals in the carbonate of foraminiferal shells are temperature-dependent and can be converted into a record of SST through the application of empirical equations. We derived SST from Mg/Ca using the calibration of Mashiotta *et al.* (9, 18). The core-top $\text{SST}_{\text{Mg/Ca}}$ estimate of 11.8°C is within the modern SST range of 8.5° to 14.5°C around the core location (19) and agrees well with a calcification of *G. bulloides* in austral spring (20). $\text{SST}_{\text{Mg/Ca}}$ on glacial-interglacial time scales ranges from 6.5° to 16°C , with mean glacial-interglacial changes in the range from 4.9° to 6.8°C (Fig. 1). On millennial time scales, $\text{SST}_{\text{Mg/Ca}}$ displays amplitudes of up to 3°C ; that is, 40 to 60% of the total glacial-interglacial amplitude (Fig. 2). The last glacial-interglacial $\text{SST}_{\text{Mg/Ca}}$ change of 4.9°C is within the range of amplitudes of 4° to 6°C that is derived

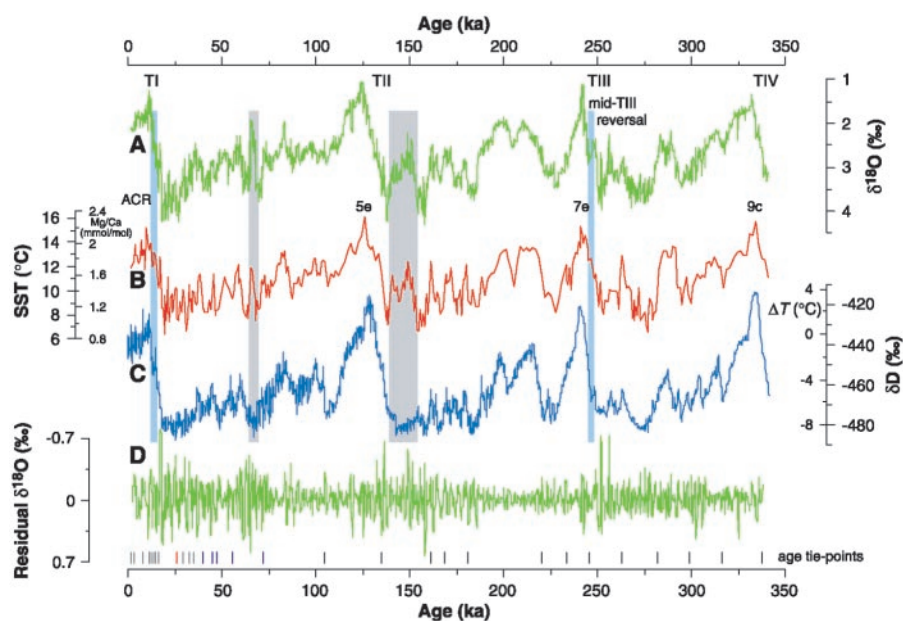


Fig. 1. 340-ky-long $\delta^{18}\text{O}_{\text{plk}}$ and $\text{SST}_{\text{Mg/Ca}}$ records from core MD97-2120 compared to the Vostok δD record (5). (A) *G. bulloides* $\delta^{18}\text{O}$ was measured at a sampling interval of 2 cm, equivalent to a time step of 192 ± 83 years. (B) $\text{SST}_{\text{Mg/Ca}}$ record (time step, 931 ± 405 years). The Mg/Ca scale is also given. Mg/Ca ratios were converted to SST using the equation of Mashiotta *et al.* (18) [$\text{Mg/Ca} = 0.474 \cdot 10^{0.107T}$ (T , temperature)]. (C) δD record (time step, 126 ± 100 years) of the Antarctic Vostok ice core on the orbitally tuned age scale of (17). Beyond ~ 230 ky, the resolution of $\delta^{18}\text{O}_{\text{plk}}$ is equal to or exceeds that of the Vostok record. δD documents air temperature changes that are indicated along the δD axis as deviations from the modern value (ΔT) (5). Vostok ΔT and our $\text{SST}_{\text{Mg/Ca}}$ are scaled to the same temperature range to facilitate comparison of both records. (D) Residual $\delta^{18}\text{O}_{\text{plk}}$ [variability ≥ 5 ky was removed from $\delta^{18}\text{O}_{\text{plk}}$ in (A)] (39). Amplitudes of the residual $\delta^{18}\text{O}_{\text{plk}}$ are systematically increased during glacial, indicating increased climate variability during periods of enhanced global ice volumes. Steep $\delta^{18}\text{O}_{\text{plk}}$ gradients labeled TI through TIV are glacial Terminations I through IV. Blue vertical bars mark the Antarctic Cold Reversal (ACR) [14 to 12.4 ky (5, 6)], and a prominent $\delta^{18}\text{O}_{\text{plk}}$ reversal in mid-Termination III. Gray vertical bars denote $\delta^{18}\text{O}_{\text{plk}}$ and $\text{SST}_{\text{Mg/Ca}}$ excursions not seen in the Vostok δD record. In contrast to the ACR, the $\delta^{18}\text{O}_{\text{plk}}$ reversal in TIII does not coincide with a drop in $\text{SST}_{\text{Mg/Ca}}$, suggesting a local seawater $\delta^{18}\text{O}_{\text{w}}$ anomaly at this time. The mid-TIII reversal is not as clearly developed in the Vostok δD record but exists as a distinct anomaly in the Vostok Ar record (29). Age control points used to construct the age model are shown along the bottom axis as follows: ^{14}C AMS dates (gray), Kawakawa tephra (red), tie points for correlating the benthic $\delta^{18}\text{O}$ section to that of northeast Atlantic core MD95-2042 (9, 16) (blue), and tie points for correlating $\text{SST}_{\text{Mg/Ca}}$ to the Vostok δD record (black).

¹School of Earth, Ocean and Planetary Sciences, Cardiff University, Park Place, Cardiff CF10 3YE, UK.

²Institució Catalana de Recerca i Estudis Avançats (ICREA) and Facultat de Geologia, Grup de Recerca Consolidat (GRC) en Geociències Marines, Departament d'Estratigrafia, Paleontologia i Geociències Marines, Universitat de Barcelona, Campus de Pedralbes, 08028 Barcelona, Spain. ³Department of Earth Sciences, University of Cambridge, Downing Street, Cambridge CB2 3EQ, UK. ⁴Department of Geosciences and DFG Research Center "Ocean Margins," University of Bremen, 28334 Bremen, Germany.

*To whom correspondence should be addressed. E-mail: pahnek@cf.ac.uk (K.P.); rainer@geo.uib.es (R.Z.)

REPORTS

from temperature-sensitive alkenones and foraminiferal census counts at nearby core sites (21, 22).

Carbonate dissolution during cold periods at our 1210-m core site (23) has the potential to lower Mg/Ca and thus the inferred SST_{Mg/Ca} (24, 25). The effect of this would be to increase the temperature amplitudes between glacial and interglacial periods. The Ca content of the sediment varies from 5 to 25%,

which by itself might imply dissolution, but there are substantial dissimilarities as well as similarities between the SST_{Mg/Ca} record and bulk sediment carbonate concentrations along the core (26). Additionally, the comparison with independent SST reconstructions from nearby cores (see above) shows good agreement: There is, at most, a 0.9°C overestimation of the last glacial-interglacial SST_{Mg/Ca}. This is much smaller than the millennial-

scale SST_{Mg/Ca} changes of up to 3°C, suggesting that the effect of any dissolution on the SST_{Mg/Ca} variability in our core is minor.

SST_{Mg/Ca} and δ¹⁸O_{plk} co-vary, with SST_{Mg/Ca} leading on average by 1.7 ± 0.3 ky, 2.2 ± 0.1 ky, and 0.8 ± 0.1 ky (90% confidence intervals) in the orbital eccentricity, obliquity, and precession bands, respectively. SST leads over planktonic δ¹⁸O values of similar magnitude have been found at low-latitude (27, 28) and Southern Ocean sites (18) and are also seen in Antarctic temperature over global ice volume (17, 29). However, the leads in our records are concentrated primarily within the cooling trends of interglacial marine isotope stage (MIS) 5e-d, MIS 7c-a, and the MIS 9a-8 transition; whereas in glacial sections and during glacial terminations, SST_{Mg/Ca} is synchronous with δ¹⁸O_{plk} (9). The variable phasing we observe between our records indicates that the contribution of local temperature and salinity effects to δ¹⁸O_{plk} varied as a function of glacial-interglacial climate.

δ¹⁸O_{plk}, like Mg/Ca, is SST-sensitive, with additional contributions coming from global ice volume and local surface water δ¹⁸O (δ¹⁸O_w) signals in δ¹⁸O_{plk}. The combined use of SST_{Mg/Ca} and δ¹⁸O_{plk} in paleotemperature equations enables us to infer δ¹⁸O_w that can then be translated into sea surface salinity (SSS) equivalents (9). The SSS record shows that salinity was systematically decreased during glacials by an average of 1.3 to 1.5 units (Fig. 3). On faster millennial time scales, salinity likewise varies at high amplitudes, around 1.2 units, with salinity decreases concentrated around stadial (cold) phases (Fig. 2). This is in apparent contrast to evidence from pollen assemblages that implies increased aridity in the region during glacials (30), from which one would expect increased evaporation-driven surface salinity. Moreover, paleoenvironmental and archaeological evidence from Australia indicates a transition from humid conditions between 50 to 40 ky to higher aridity between 40 to 30 ky (31). Our SSS record shows several maxima during this time span, but they all occur before a background of decreased SSS (Fig. 2). A viable modulator of regional surface salinity that operates independently from evaporation and precipitation is the hydrographic gradient associated with the circum-Antarctic ocean fronts that separate warmer, more saline surface waters to the north from colder, fresher waters to the south. Northward migration of the mobile fronts during glacial and stadial periods is a plausible means by which the core site was brought under the influence of fresher sub-antarctic surface waters (23). Sporadic meltwater surges from South Island, New Zealand, and melting Antarctic icebergs have contributed to the observed salinity anomalies on subor-

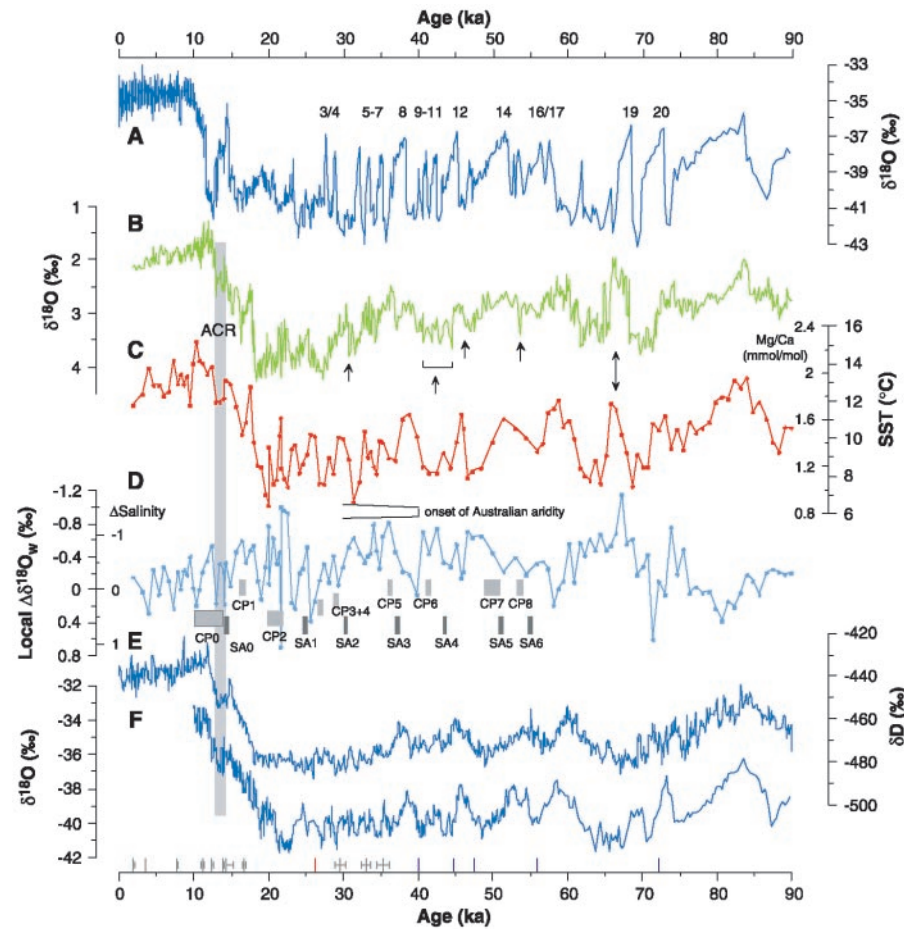


Fig. 2. δ¹⁸O_{plk}, SST_{Mg/Ca}, and local δ¹⁸O_w records of core MD97-2120 compared to the Greenland GISP2 δ¹⁸O_{ice} record and the Antarctic Vostok and Byrd ice core records for the past 90 ky. (A) δ¹⁸O_{ice} record from GISP2 (2). Numbers denote D/O interstadials during MIS 3. (B) δ¹⁸O_{plk} record of core MD97-2120. (C) SST_{Mg/Ca} record. A Mg/Ca scale is given along the SST axis. (D) Local δ¹⁸O_w anomaly as derived from δ¹⁸O_{plk} and SST_{Mg/Ca} after correcting δ¹⁸O_{plk} for mean ocean δ¹⁸O_w changes (9, 32). For δ¹⁸O_w calculation, δ¹⁸O_{plk} was sampled at the time step of the lower-resolution SST_{Mg/Ca} record. The δ¹⁸O_w anomaly was calculated using the mean Holocene (0 to 6 ky) value as a reference. The equivalent salinity anomaly (the inside scale along the δ¹⁸O_w axis) is based on a δ¹⁸O_w-salinity relation for high southern latitudes (9). The onset and trend of increasing Australian aridity at 40 ky are from (37). Control points along bottom axis were used to construct the age model as in Fig. 1, now with error bars of the calibrated ¹⁴C ages. (E and F) Antarctic Vostok δD (5) and Byrd δ¹⁸O_{ice} ice core records (6) are shown for comparison. Single-headed arrows along the δ¹⁸O_{plk} record in (B) denote rapid transitions and short events not seen in Antarctic ice core records. The double-headed arrow in (B) marks the large δ¹⁸O_{plk} and SST_{Mg/Ca} excursion during MIS 4, which is not present in the Vostok δD record. The event immediately follows the warm anomaly in Byrd at ~70 ky and partly overlaps with the Greenland D/O 19 event. Bars along the δ¹⁸O_w anomaly in (D) indicate increased IRD delivery on Campbell Plateau (CP0 to CP8), south of Chatham Rise (48° to 53°S) (34), and in the South Atlantic at 41° and 53°S (SA0 to SA6) (33). SA0 and CP0 are coeval with the ACR and coincide in our SSS record with a discrete minimum. SA1 to SA4 are associated directly with, or are on the shoulders of, SSS minima. The off-SSS-peak positions of some SA events are due to age model uncertainty. Linking with times of increased IRD delivery on Campbell Plateau (CP1-6) is more direct because of proximity to our core site; these phases correspond to SSS minima. SA5 and SA6 and CP7 and CP8 are exceptional in that they correlate with a broad SST_{Mg/Ca} maximum in our record but with only moderately increased SSS.

bital time scales. By applying a modern $\delta^{18}\text{O}_w$ -salinity relation, we may overestimate the amplitude of salinity changes to some extent, because increased oxygen isotope fractionation during precipitation at low glacial temperatures and an influence of low- $\delta^{18}\text{O}_w$ meltwaters from Antarctica and disintegrating New Zealand glaciers have likely altered the $\delta^{18}\text{O}_w$ -salinity relation. We also note that the mean ocean $\delta^{18}\text{O}_w$ record (32) that we used to correct $\delta^{18}\text{O}_{\text{plk}}$ for global ice volume effects does not offer true millennial-scale resolution, which introduces uncertainty in the range of 0.2 to 0.3 salinity units (9). But these factors do not alter the overall picture of low SSS during cold periods. In fact, some of the minima along our SSS record are coeval with ice-rafted debris (IRD) events in the South Atlantic and on Campbell Plateau, south of Chatham Rise (Fig. 2) (33, 34), which in turn demonstrates the importance of these events for the wider circum-Antarctic region.

The high temporal resolution and fine structure of the $\delta^{18}\text{O}_{\text{plk}}$ and $\text{SST}_{\text{Mg/Ca}}$ profiles of core MD97-2120 allow for a detailed comparison with Antarctic ice core climate records. On orbital time scales, our records directly mirror the structure of the Vostok δD record, which reflects air temperature changes over Antarctica (5) (Fig. 1). The similarities, for instance, hold for the interglacial peak heights (MIS 5e, 7e, and 9e), which in both records exceed Holocene levels. Temperature amplitudes across Terminations I to III are higher in the Vostok record (9.5°, 12.3°, and 9.3°C) than in $\text{SST}_{\text{Mg/Ca}}$ (8.8°, 8.9°, and 7.2°C), which indicates strong Antarctic cooling during glacials in connection with increased thermal isolation due to enhanced circum-Antarctic circulation (35). During Termination I, $\delta^{18}\text{O}_{\text{plk}}$ and $\text{SST}_{\text{Mg/Ca}}$ display a brief reversal of 0.6 per mil (‰) and 1.1°C, respectively, that is similar in structure and timing to the 1.9°C cooling during the Antarctic Cold Reversal in the Vostok and Byrd ice core records (5, 6) (Fig. 2). A similar short-lived $\delta^{18}\text{O}_{\text{plk}}$ reversal is developed during Termination III (250 to 242 ky) that is likewise documented in the Vostok δD and argon records (5, 29) (Fig. 1). The mid-Termination III reversal is covered by five data points in our $\text{SST}_{\text{Mg/Ca}}$ record that show a transient halt in the warming trend but no coeval $\text{SST}_{\text{Mg/Ca}}$ decrease. This suggests that the $\delta^{18}\text{O}_{\text{plk}}$ reversal reflects the incursion of a short-lived local salinity maximum (Fig. 3).

Dissimilarity exists with the Antarctic ice core record during glacial periods in that $\delta^{18}\text{O}_{\text{plk}}$ shows enhanced variability with abrupt transitions that are not seen in the ice cores (Figs. 1 and 2). Some short-lived $\delta^{18}\text{O}_{\text{plk}}$ and $\text{SST}_{\text{Mg/Ca}}$ changes are reminiscent of the glacial climatic oscillations recorded in Northern Hemisphere records (1, 2,

16) (Fig. 2). For instance, the sequence of $\delta^{18}\text{O}_{\text{plk}}$ anomalies between 46 and 41 ky mimics the structure of Dansgaard/Oeschger (D/O) events 9 to 12 in the Greenland ice core record (Fig. 2). The pronounced $\text{SST}_{\text{Mg/Ca}}$ warm anomaly during MIS 6 (154 to 138 ky) reaches a maximum amplitude of 5.7°C and is mirrored by a coeval negative $\delta^{18}\text{O}_{\text{plk}}$ anomaly of 1.8‰. A similar anomaly is documented in North Atlantic (36) and tropical Pacific (28) marine records, but is absent from the Vostok record. It coincides with an orbital precession minimum and hence a maximum in Northern Hemisphere insolation, suggesting northern forcing as the cause for the warm anomaly. The likewise pronounced $\text{SST}_{\text{Mg/Ca}}$ excursion of 4.4°C during MIS 4, between 68.3 and 65.6 ky, is mirrored by a 1.6‰ $\delta^{18}\text{O}_{\text{plk}}$ decrease that is not developed in the benthic $\delta^{18}\text{O}$ section of our core (9). This event on our age scale immediately follows the 70-ky warm anomaly in the Byrd ice core record but overlaps with D/O event 19 (69 to 66 ky) in Greenland (Fig. 2).

On glacial-interglacial time scales, our records show a varying degree of similarity with the paleoclimate record from Antarctic ice cores. Evidently, the degree of climatic coupling of mid-southern latitudes to Antarctica changed as a function of global climate, requiring a mechanism that perturbs this climatic link during cold intervals. Varying Antarctic Cir-

cumpolar Current (ACC) intensity, as an indirect response to variations in westerly wind strength (37), provides for such a mechanism in that the ACC modulates the transmission of climate signals across high southern latitudes (38). In response to stronger decoupling from Antarctic climate, the mid-latitude Southern Hemisphere was more likely to be influenced by climatic oscillations and abrupt transitions not felt in Antarctica. A significant increase in the amplitude of $\delta^{18}\text{O}_{\text{plk}}$ during glacial periods of the past 340 ky becomes apparent in the $\delta^{18}\text{O}_{\text{plk}}$ record, when variability ≥ 5 ky is removed from the data (39) (Fig. 1). This provides clear evidence that the magnitude of millennial-scale climatic oscillations is dependent on the state of the global climate, notably the presence of large ice sheets in the Northern Hemisphere (40).

Paleoclimatic records from various archives in the Southern Hemisphere have been used to infer both interhemispheric synchrony and asynchrony (6, 27, 41–43). However, radiocarbon dating and the uncertainty related to variations of local reservoir ages (9, 13), as well as graphical tuning of the records to other paleorecords, do not offer the control needed for robust assessment of interhemispheric temporal patterns of climate change. For instance, we can fit parts of the glacial sections of our $\delta^{18}\text{O}_{\text{plk}}$ record to the Greenland $\delta^{18}\text{O}$ record without violating the graph-

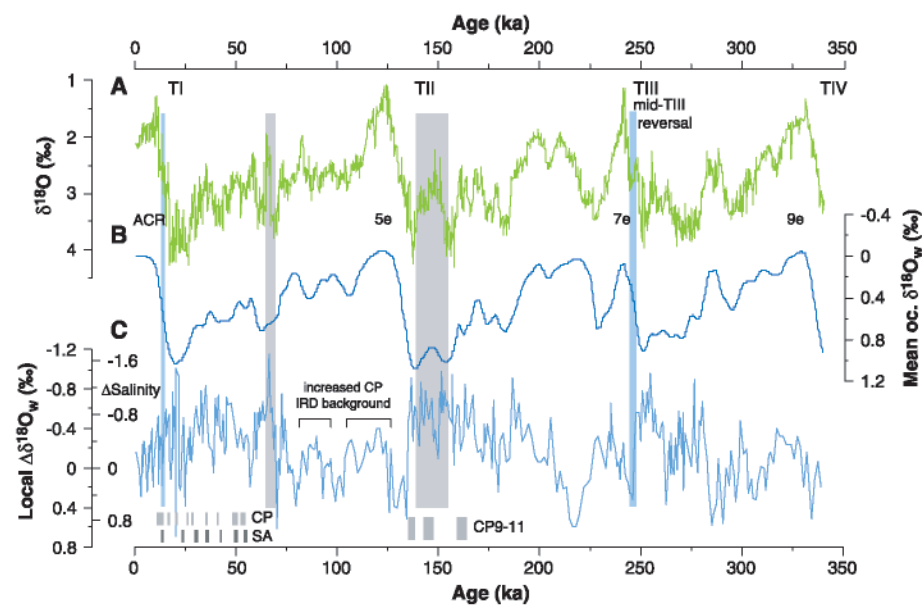


Fig. 3. $\delta^{18}\text{O}_{\text{plk}}$ of core MD97-2120 and mean ocean $\delta^{18}\text{O}_w$ (32) used to estimate local $\delta^{18}\text{O}_w$ and SSS changes. (A) $\delta^{18}\text{O}_{\text{plk}}$ record. (B) Mean ocean $\delta^{18}\text{O}_w$ record (32) used to correct $\delta^{18}\text{O}_w$ for global ice volume changes. (C) Local $\delta^{18}\text{O}_w$ and salinity anomalies as in Fig. 2, here for the past 340 ky. Blue and gray vertical bars mark events as described in Fig. 1. Bars along the bottom age scale refer to periods of enhanced IRD delivery on Campbell Plateau (CP), south of Chatham Rise (34), and in the South Atlantic (SA) (33); CP9 and CP10 coincide with low-SSS anomalies that are interrupted by short excursions to higher SSS values. The broad salinity minima at 96 to 84 ky and 125 to 110 ky coincide with meltwater surges between 80 and 130 ky as described in (34). Provenance studies on Campbell Plateau suggest an Antarctic origin for the IRD (34). A glacially intensified Southland Current flowing northeastward along South Island would have isolated Campbell Plateau from local iceberg drifts and meltwater surges from South Island. These may have reached Chatham Rise, thus causing recurrent low-SSS anomalies during glacial periods.

REPORTS

ical correlation between the benthic $\delta^{18}\text{O}$ sections of our core and core MD95-2042 from the northeast Atlantic (16). Thus, our age model is consistent with, but cannot prove, a direct mechanistic connection and synchrony between the short-lived excursions in our $\delta^{18}\text{O}_{\text{plk}}$ record and rapid Northern Hemisphere D/O events.

A notable implication from our study is that extrapolar climates in the Southern Hemisphere were more variable than is inferred on the basis of Antarctic ice cores alone. Intensified circumpolar ocean and atmospheric circulation during glacials increasingly isolated Antarctica from extrapolar climates, which therefore are not adequately represented in Antarctic paleoclimate records. The similarity of our $\delta^{18}\text{O}_{\text{plk}}$ record with D/O cycles in Greenland that is evident in some glacial sections is suggestive of direct climatic linking and synchrony between the hemispheres.

References and Notes

- W. Dansgaard *et al.*, *Nature* **364**, 218 (1993).
- P. M. Grootes, M. Stuiver, *J. Geophys. Res.* **102**, 26455 (1997).
- G. Bond *et al.*, *Science* **278**, 1257 (1997).
- J. P. Sachs, S. J. Lehman, *Science* **286**, 756 (1999).
- J. R. Petit *et al.*, *Nature* **399**, 429 (1999).
- T. Blunier, E. J. Brook, *Science* **291**, 109 (2001).
- See the IMAGES Web site at <http://images.pclab.ifg.uni-kiel.de>.
- R. A. Heath, *N. Z. J. Mar. Freshw. Res.* **19**, 79 (1985).
- Methods are available as supporting online material on Science Online.
- C. J. N. Wilson, V. R. Switsur, A. P. Ward, *Geol. Mag.* **125**, 297 (1988).
- L. Carter, H. L. Neil, I. N. McCave, *Palaeogeogr. Palaeoclimatol. Palaeoecol.* **162**, 333 (2000).
- M. Stuiver *et al.*, *Radiocarbon* **40**, 1041 (1998).
- E. L. Sikes, C. R. Samson, T. P. Guilderson, W. R. Howard, *Nature* **405**, 555 (2000).
- A. H. L. Voelker, P. M. Grootes, M. J. Nadeau, M. Sarnthein, *Radiocarbon* **42**, 437 (2000).
- C. Laj *et al.*, *Earth Planet. Sci. Lett.* **200**, 177 (2002).
- N. J. Shackleton, M. A. Hall, E. Vincent, *Paleoceanography* **15**, 565 (2000).
- N. J. Shackleton, *Science* **289**, 1897 (2000).
- T. A. Mashioita, D. W. Lea, H. J. Spero, *Earth Planet. Sci. Lett.* **170**, 417 (1999).
- M. J. Uddstrom, N. A. Oien, *J. Geophys. Res.* **104**, 20729 (1999).
- A. L. King, W. R. Howard, *Deep-Sea Res.* **48**, 1687 (2001).
- P. Wells, H. Okada, *Mar. Micropaleontol.* **32**, 341 (1997).
- E. L. Sikes, W. R. Howard, H. L. Neil, J. K. Volkman, *Paleoceanography* **17**, 10.1029/2001PA000640 (2002).
- P. P. E. Weaver, L. Carter, H. L. Neil, *Paleoceanography* **13**, 70 (1998).
- S. J. Brown, H. Elderfield, *Paleoceanography* **11**, 543 (1996).
- Y. Rosenthal, G. P. Lohmann, K. C. Lohmann, R. M. Sherrell, *Paleoceanography* **15**, 135 (2000).
- K. Pahnke, R. Zahn, H. Elderfield, M. Schulz, data not shown.
- E. Bard, F. Rostek, C. Sonzogni, *Nature* **385**, 707 (1997).
- D. W. Lea, D. K. Pak, H. J. Spero, *Science* **289**, 1719 (2000).
- N. Caillon *et al.*, *Science* **299**, 1728 (2003).
- L. E. Heusser, G. van de Geer, *Quat. Sci. Rev.* **13**, 273 (1994).
- J. M. Bowler *et al.*, *Nature* **421**, 837 (2003).
- C. Waelbroeck *et al.*, *Quat. Sci. Rev.* **21**, 295 (2002).
- S. L. Kanfoush *et al.*, *Science* **288**, 1815 (2000).
- L. Carter, H. L. Neil, L. Northcote, *Mar. Geol.* **191**, 19 (2002).
- M. D. Cox, *J. Phys. Oceanogr.* **19**, 1730 (1989).
- J. F. McManus, D. W. Oppo, J. L. Cullen, *Science* **283**, 971 (1999).
- D. Borowski, R. Gerdes, D. Olbers, *J. Phys. Oceanogr.* **32**, 2520 (2002).
- A. Schmittner, O. A. Saenko, A. J. Weaver, *Quat. Sci. Rev.* **22**, 659 (2003).
- We isolated the high-frequency variability from the planktonic $\delta^{18}\text{O}$ record using a high-pass filter with cutoff frequency of 1/(5 ky). Before filtering, the data were evenly sampled at 190-year intervals.
- M. Schulz, W. H. Berger, M. Sarnthein, P. M. Grootes, *Geophys. Res. Lett.* **26**, 3385 (1999).
- C. D. Charles, S. J. Lynch, U. S. Ninnemann, R. G. Fairbanks, *Earth Planet. Sci. Lett.* **142**, 19 (1996).
- G. H. Denton *et al.*, *Geogr. Ann.* **81 A**, 107 (1999).
- A. Mazaud *et al.*, *Earth Planet. Sci. Lett.* **201**, 159 (2002).
- We thank G. Bianchi, Cardiff, for running the mass spectrometer; M. Greaves, Cambridge, for assistance with the Mg/Ca analyses; and P. Grootes and M. Nadeau for the ^{14}C AMS datings. K.P. and R.Z. acknowledge financial support from the Leverhulme Trust, UK, under grant F/407/J. H.E. thanks the Natural Environment Research Council for financial support (grant GR3/1308). This is contribution number 6 of the School of Earth, Ocean and Planetary Sciences, Cardiff University.

Supporting Online Material

www.sciencemag.org/cgi/content/full/301/5635/948/DC1

Materials and Methods

Figs. S1 to S3

Tables S1 and S2

References

12 March 2003; accepted 17 July 2003

Coral Reef Death During the 1997 Indian Ocean Dipole Linked to Indonesian Wildfires

Nerilie J. Abram,^{1*} Michael K. Gagan,¹ Malcolm T. McCulloch,¹ John Chappell,¹ Wahyoe S. Hantoro²

Geochemical anomalies and growth discontinuities in *Porites* corals from western Sumatra, Indonesia, record unanticipated reef mortality during anomalous Indian Ocean Dipole upwelling and a giant red tide in 1997. Sea surface temperature reconstructions show that although some past upwelling events have been stronger, there were no analogous episodes of coral mortality during the past 7000 years, indicating that the 1997 red tide was highly unusual. We show that iron fertilization by the 1997 Indonesian wildfires was sufficient to produce the extraordinary red tide, leading to reef death by asphyxiation. These findings highlight tropical wildfires as an escalating threat to coastal marine ecosystems.

Coral reefs, the most diverse of all marine ecosystems, are increasingly threatened by human activities, climate change, and disease (1–3). The exact nature and potential impact of these threats are still unclear in many cases, making effective conservation difficult. The vulnerability of reefs to climate change became fully evident in 1997–1998 when elevated sea surface temperatures (SSTs) linked to global warming and a strong El Niño caused widespread coral bleaching and mortality throughout the tropical oceans (3–5). Bleaching was particularly severe in the central and western Indian Ocean, where approximately 59% of reefs were damaged, creating large socioeconomic problems (3). Although SSTs in the central-western tropical Indian Ocean were anomalously warm during 1997, the eastern sector was unusually cool. These cool SSTs were the result of recently

discovered coupled ocean-atmosphere dynamics (6, 7), termed the Indian Ocean Dipole (IOD). The anomalously cool SSTs in the eastern Indian Ocean during 1997, together with the economic and political crisis in Indonesia at this time, led to the status of coral reefs in western Indonesia being largely overlooked during systematic surveys of the 1997–1998 coral bleaching event.

Here, we report on the unanticipated and catastrophic death in late 1997 of the Mentawai Islands reef ecosystem, located offshore of southwest Sumatra, Indonesia, in the equatorial eastern Indian Ocean (Fig. 1). Before 1997, more than 101 species of hard corals (8), including centuries-old colonies of *Porites* (9, 10), provided a diverse reef ecosystem around the Mentawai Islands. During the 1997 IOD, enhanced southeasterly trade winds drove strong upwelling along the southwest coast of Sumatra, causing SSTs in the Mentawai reefs to drop by around 4°C (Fig. 1) (6, 7). At the same time, convective rainfall over Indonesia was dramatically reduced, and wildfires produced thick smoke coverage over southeast Asia (6, 7). In late 1997, near the peak of the IOD, close to 100% of

¹Research School of Earth Sciences, The Australian National University, Canberra, ACT 0200, Australia.

²Research and Development Center for Geotechnology, Indonesian Institute of Sciences (LIPI), Bandung, 40135, Indonesia.

*To whom correspondence should be addressed. E-mail: nerilie.abram@anu.edu.au